

Supplemental text, figures, and tables

”High resolution reconstructions of the Southwest Indian Ridge, 52 Ma to present: Implications for the breakup and absolute motion of the Africa plate”

by C. DeMets, S. Merkouriev, & D. Sauter

Overview

This supplementary document includes 21 figures and one table, all of which are referenced in the main document. Figures 9 through 21 are maps of the high-resolution bathymetry, along-track magnetic anomaly observations, and our magnetic reversal and fracture zone interpretations and reconstructions. All the maps are meant to be viewed at large scale for readers who desire a synoptic view of the data, interpretations, and fits. All the magnetic reversal and fracture zone crossings used in the analysis and displayed on the maps can be accessed at marine-geo.org.

List of supplementary contents

1. *Supplemental Figure 1*: A synthetic magnetic anomaly profile for the central Southwest Indian Ridge and all 44 specific reversal tie points that were correlated for our reconstructions. Half of the 44 tie points are identified to the left of the central anomaly at 0 Myr and the other to the right. The ages for each tie point are given in Table 1 of the main document.
2. *Supplemental Figure 2*: Comparisons of the weighted r.m.s. misfits for all three plate pairs along the Southwest Indian Ridge for each of the 44 times for which the data were reconstructed across the ridge and the w.r.m.s. misfit for Chron 1n to 13 reconstructions of magnetic reversals and fracture zones for the Nubia-South America plate pair in the southern and central Atlantic basin (DeMets & Merkouriev 2019). Misfits for the Nubia-South plate pair were selected for comparison to the misfits reported in this study due to the similarity of the southern Atlantic basin spreading rates to the Southwest Indian Ridge and high quality of the data-rich reconstructions for the southern and central Atlantic.
3. *Supplemental Figures 3-5*: Summary fits of predicted and digitized fracture zone traces for the Nubia-Antarctic (Supplemental Figure 3), Lwandle-Antarctic (Supplemental Figure 4), and Somalia-Antarctic (Supplemental Figure 5) plate pairs. The distances and/or age of zero in each figure corresponds to the northern and southern intersections between the ridge axis and transform fault, which is the seed point for the predicted flow line.
4. *Supplemental Figure 6*: Evidence for a significant clockwise rotation of the abyssal hill fabric orientation at the time of Chron 18 along the Lwandle-Antarctic plate boundary north of the ridge. The sense and timing of the fabric reorientation agree with that for the Somalia-Antarctic plate boundary (see Fig. 13 and discussion in the main document).
5. *Supplemental Figure 7*: Absence of evidence for a major change in the abyssal hill fabric orientation at the time of Chron 18 along the Nubia-Antarctic plate boundary north of the ridge. The relatively unchanged orientations of the abyssal hill before and after Chron 18 differs from the more obvious seafloor fabric reorientation at this time at 59°E along the Somalia-Antarctic segment (Fig. 14 of the main document).

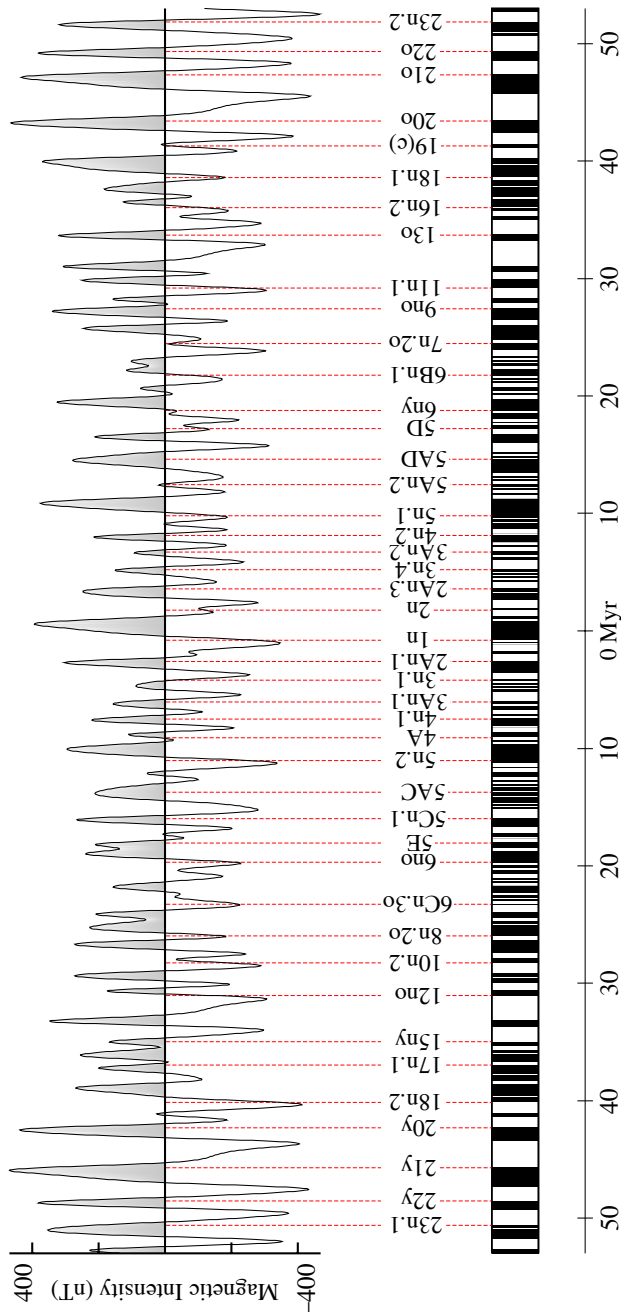
6. *Supplemental Figure 8*: Comparison of C1n to C23 finite pole locations for all three plate pairs as estimated from the REDBACK analyses of their best-fitting rotation sequences. The pole locations for the Lwandle-Antarctic and Somalia-Antarctic plate pairs are remarkably similar even though the two were derived from magnetic reversal and fracture zone crossings from two different areas of the Southwest Indian Ridge. The Nubia-Antarctic pole path and locations differs from those for the other two plate pairs, consistent with significant movement of the western portion of the Africa plate (Nubia) relative to its eastern portion (Lwandle and Somalia) since at least 40 Ma.
7. *Supplemental Figure 9 (large scale map)*: Synthesis of French bathymetric grids that were used to identify fracture zones and transform faults for portions of the analysis focused on the ridge east of 54°E. Grids are depicted at their maximum ≈ 100 meter resolution. Red lines that are apparent on magnification of the figure show the locations of abyssal hills that were identified and digitized for the seafloor lineation analysis that is described in the main document. A few multibeam tracks that were not incorporated in this grid are instead available through the GeoMapApp database and were also used for our lineation analysis.
8. *Supplemental Figures 10-21 (large scale maps)*: Due to the large geographic area spanned by the Southwest Indian Ridge and the abundance of data in many areas, large scale maps of the original, along-track magnetic anomaly data, seafloor bathymetry, and our magnetic reversal and fracture zone identifications are provided for six overlapping regions along the ridge. Two maps for each region are provided, each of which shows our identifications and reconstructions for 22 of the 44 times that were selected for our study. The reversal crossings that are in their original locations are shown by large solid or large white-filled symbols. The reversal crossings that have been rotated from their location on the opposite plate use the same color scheme, but have yellow filling. A legend at the top of each figure identifies the color and symbol that are used to identify the reversal crossings for each time. Reconstructions are done with the best-fitting rotations from Tables 2, 5, and 8 in the main document. The small white circles show the digitized fracture zone flow lines described in the main document. The synthetic flow lines constructed with our best-fitting rotations are shown by the small colored circles near the digitized fracture zones. The thin red lines show the synthetic flow lines constructed with the noise-reduced rotations in Tables 3, 6, and 9 in the main document.
9. *Supplemental Table 1*: Nubia-Somalia finite rotations derived by combining Nubia-Antarctic and Somalia-Antarctic noise-reduced rotations in Tables 3 and 6 in the main document.

Supplemental Table 1. Nubia-Somalia rotations

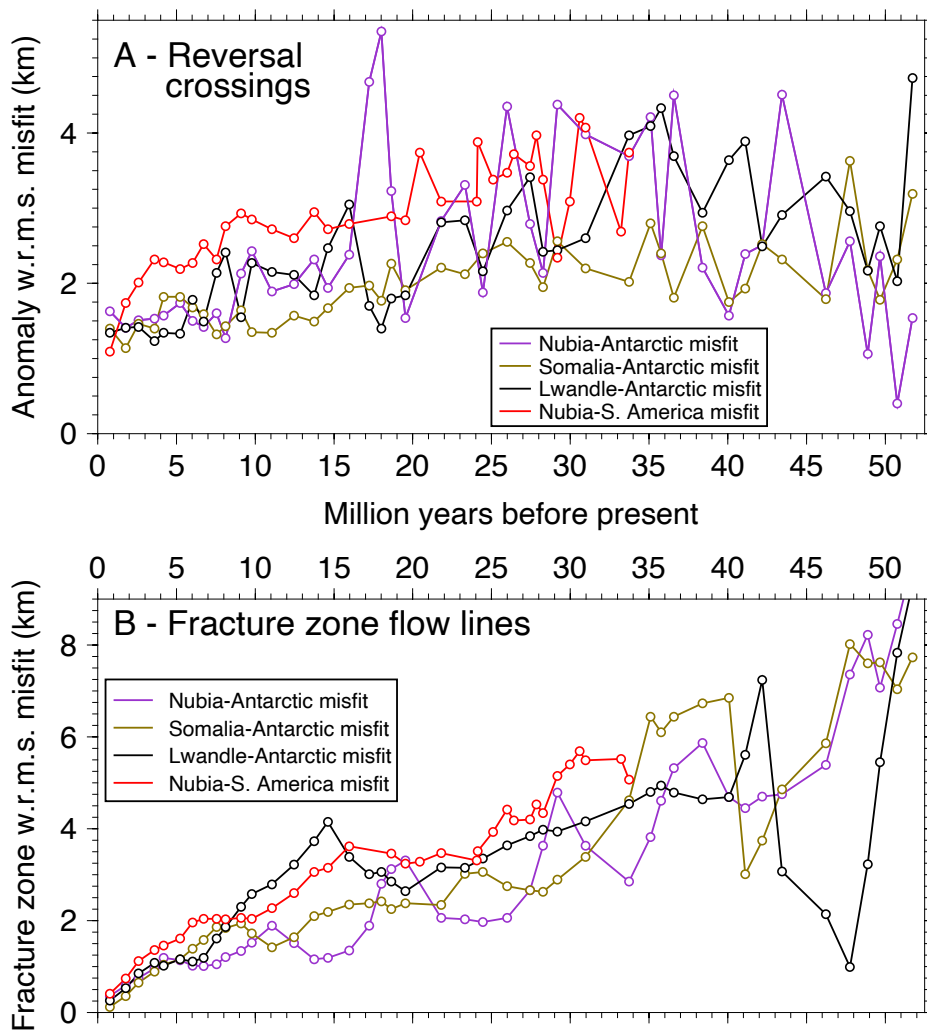
Chron	Lat. (°N)	Long. (°E)	Ω (degrees)	Covariances					
				a	b	c	d	e	f
1n	-36.70	353.48	0.028	351.2	-275.9	353.5	228.1	-296.5	387.1
2n	-43.63	1.63	0.077	398.4	-290.9	364.8	244.2	-317.9	418.2
2An.1	-47.54	7.13	0.126	436.2	-297.7	366.3	254.2	-331.3	438.8
2An.3	-49.83	10.67	0.190	498.2	-299.7	356.6	268.5	-351.6	470.8
3n.1	-49.64	10.25	0.219	530.8	-301.0	351.8	275.4	-361.3	486.0
3n.4	-47.91	7.68	0.253	506.5	-286.4	331.1	261.5	-343.5	465.0
3An.1	-46.44	5.93	0.271	509.0	-277.2	315.3	257.1	-338.6	461.0
3An.2	-45.28	4.94	0.288	555.8	-278.4	307.2	266.8	-352.7	483.6
4n.1	-44.66	5.11	0.314	598.3	-285.0	308.4	277.4	-367.0	505.0
4n.2	-44.82	6.30	0.335	620.3	-291.6	313.9	285.6	-378.1	521.1
4A	-45.12	8.41	0.374	637.1	-291.6	310.0	292.9	-389.1	539.1
5n.1	-45.21	9.67	0.403	663.6	-296.4	311.7	301.5	-401.2	557.7
5n.2	-45.14	11.56	0.460	744.9	-315.0	323.0	324.5	-432.5	604.4
5An.2	-44.54	12.48	0.537	839.1	-333.4	332.3	347.3	-463.9	651.6
5AC	-43.37	11.97	0.620	872.1	-289.1	259.1	350.8	-476.7	685.2
5AD	-42.52	11.55	0.680	965.0	-261.6	203.3	375.0	-516.5	753.8
5Cn.1	-41.13	10.75	0.777	1295.3	-257.7	148.1	465.1	-649.0	957.8
5D	-39.74	9.90	0.853	1842.2	-321.5	163.3	615.0	-859.3	1264.9
5E	-38.90	9.50	0.874	2266.1	-330.4	115.8	750.0	-1054.7	1557.8
6ny	-37.46	8.10	0.849	2426.3	-305.0	44.6	816.8	-1158.7	1727.1
6no	-33.63	3.98	0.725	2495.6	-211.3	-173.0	825.9	-1214.8	1900.0
6Bn.1	-36.76	7.57	0.697	1881.4	-366.8	149.1	652.3	-931.1	1431.5
6Cn.3	-38.45	8.35	0.754	1924.6	-350.1	105.8	662.5	-953.9	1484.6
7n.2	-40.41	10.09	0.797	2077.4	-365.6	88.4	701.3	-1014.6	1592.6
8n.2	-43.48	13.52	0.859	2378.6	-385.3	37.2	762.1	-1113.3	1779.0
9no	-45.49	15.42	0.937	2672.8	-361.2	-85.9	811.7	-1205.4	1974.4
10n.2	-46.30	15.95	0.989	2893.4	-376.5	-119.5	866.0	-1292.6	2131.8
11n.1	-47.03	16.38	1.052	3205.6	-457.9	-60.5	964.9	-1435.6	2353.8
12no	-48.20	17.24	1.203	3631.5	-385.3	-299.5	1050.9	-1598.0	2697.2
13o	-49.31	17.07	1.468	4301.9	91.1	-1296.1	1073.1	-1764.1	3264.0
15ny	-50.85	19.25	1.582	4696.6	334.2	-1807.7	1114.1	-1892.8	3611.5
16n.2	-51.80	20.99	1.634	5076.9	395.2	-2016.3	1188.4	-2032.1	3903.2
17n.1	-52.98	23.41	1.695	6016.5	157.4	-1896.9	1535.6	-2535.7	4705.2
18y	-52.89	21.89	1.828	6641.1	789.1	-3135.0	1432.0	-2547.9	5094.1
18o	-51.26	19.43	1.908	7298.7	1186.9	-3953.7	1464.4	-2717.7	5599.9
19c	-50.47	20.50	1.922	7766.9	1384.5	-4378.3	1525.7	-2870.9	5951.3
20y	-49.53	22.17	1.924	8534.7	1658.8	-5044.2	1602.8	-3078.5	6484.9
20o	-48.72	25.02	1.915	9917.1	2035.3	-6111.6	1740.8	-3428.7	7418.1

These rotations, which reconstruct the movement of the Somalia plate relative to the Nubia plate, were determined from Nubia-Antarctica and Somalia-Antarctica noise-reduced rotations in Tables

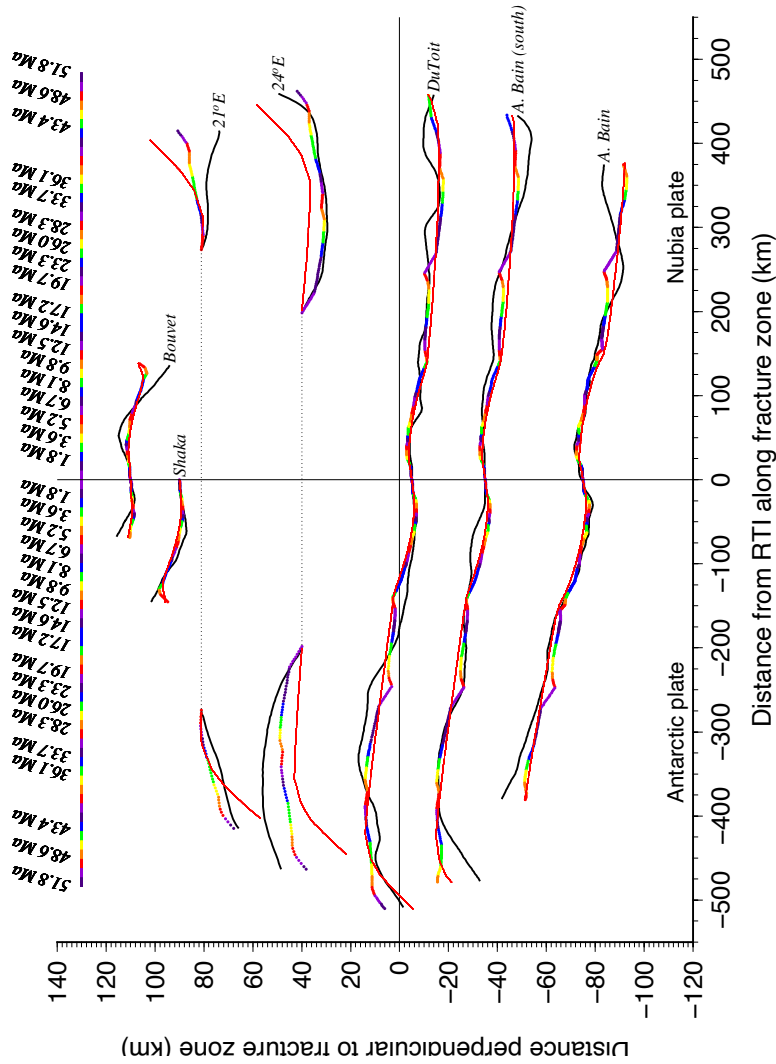
3 and 6 of the main document. The rotation angles Ω are positive anticlockwise. The Cartesian rotation covariances are calculated in a Somalia-fixed reference frame and have units of 10^{-9} radians².



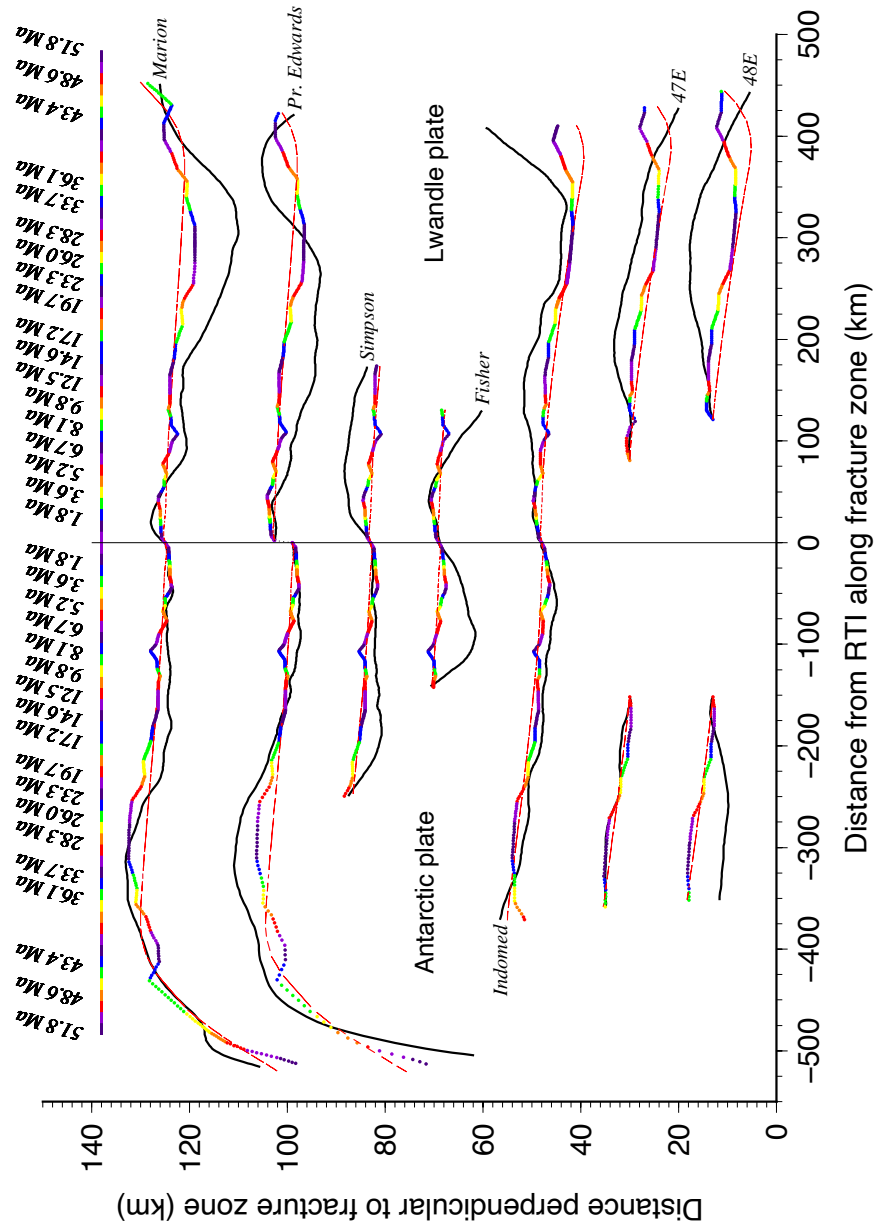
Supplemental Figure 1. Magnetic reversal correlation points (labeled dotted lines) and magnetic block model used for the study. The synthetic magnetic profile, which is appropriate for correlating magnetic anomalies along much of the central Southwest Indian Ridge, was created using a 18 mm yr^{-1} spreading rate, a ridge azimuth of $\text{N}86^\circ\text{E}$, a 1.5-km -wide reversal transition zone, and ambient and paleomagnetic inclinations and declinations for a point at 44.5°S , 37°E .



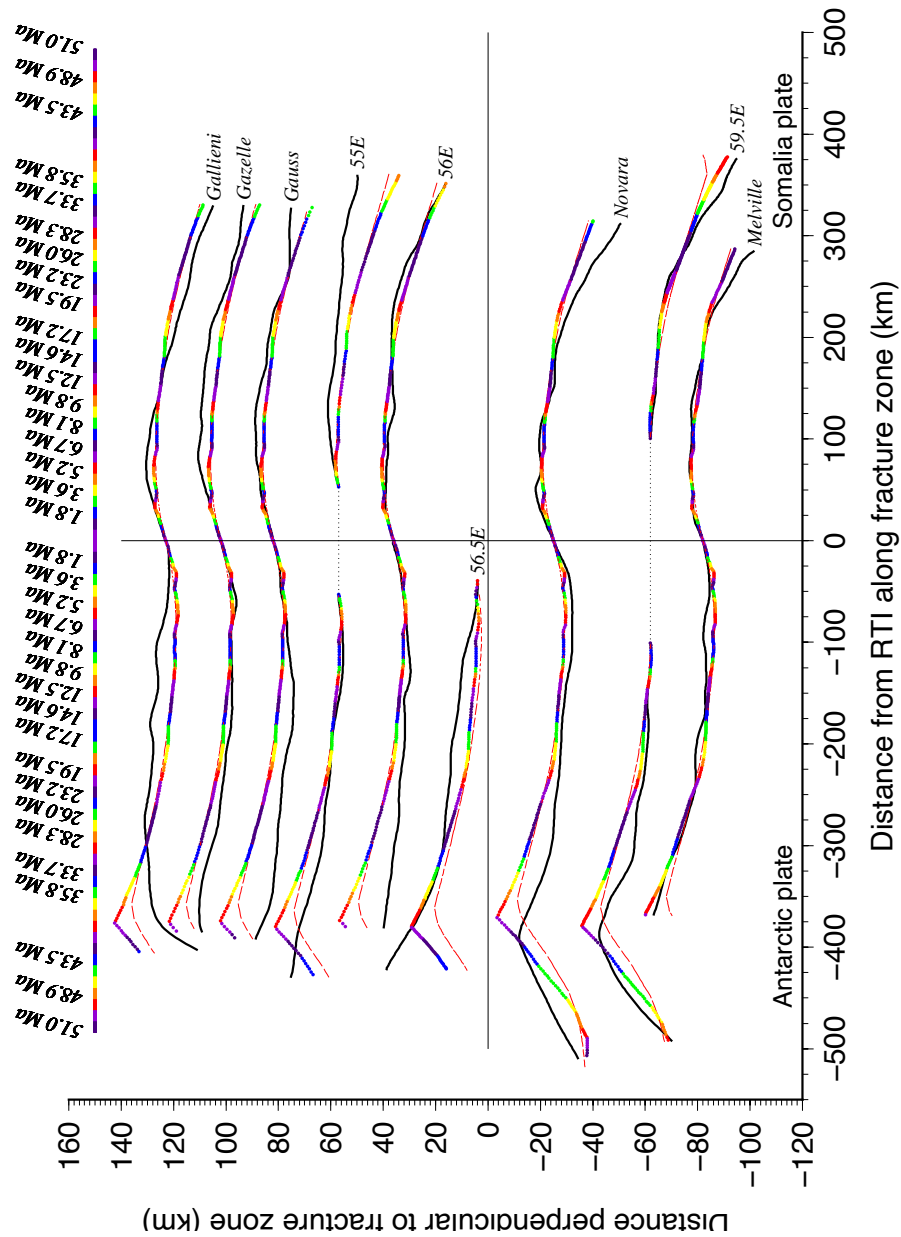
Supplemental Figure 2. Comparative weighted root-mean-square (w.r.m.s.) misfits for reconstructed magnetic reversal and fracture zones by reversal age (panel A) and fracture zone age (Panel B) per Southwest Indian Ridge plate pair and for the Nubia-South America plate pair (DeMets & Merkouriev 2019). All misfits are for reconstructions by the best-fitting rotations described in the text. The SWIR reconstruction misfits are comparable to those for the well-studied southern Mid-Atlantic Ridge, where seafloor spreading rates and the fidelities of the magnetic reversal sequences are approximately the same. The large misfit increase for the Nubia-Antarctic reversal crossings for 20-16 Ma is attributable to difficulties in identifying the sparsely surveyed magnetic anomalies for this period from the western third of the Southwest Indian Ridge (see text).



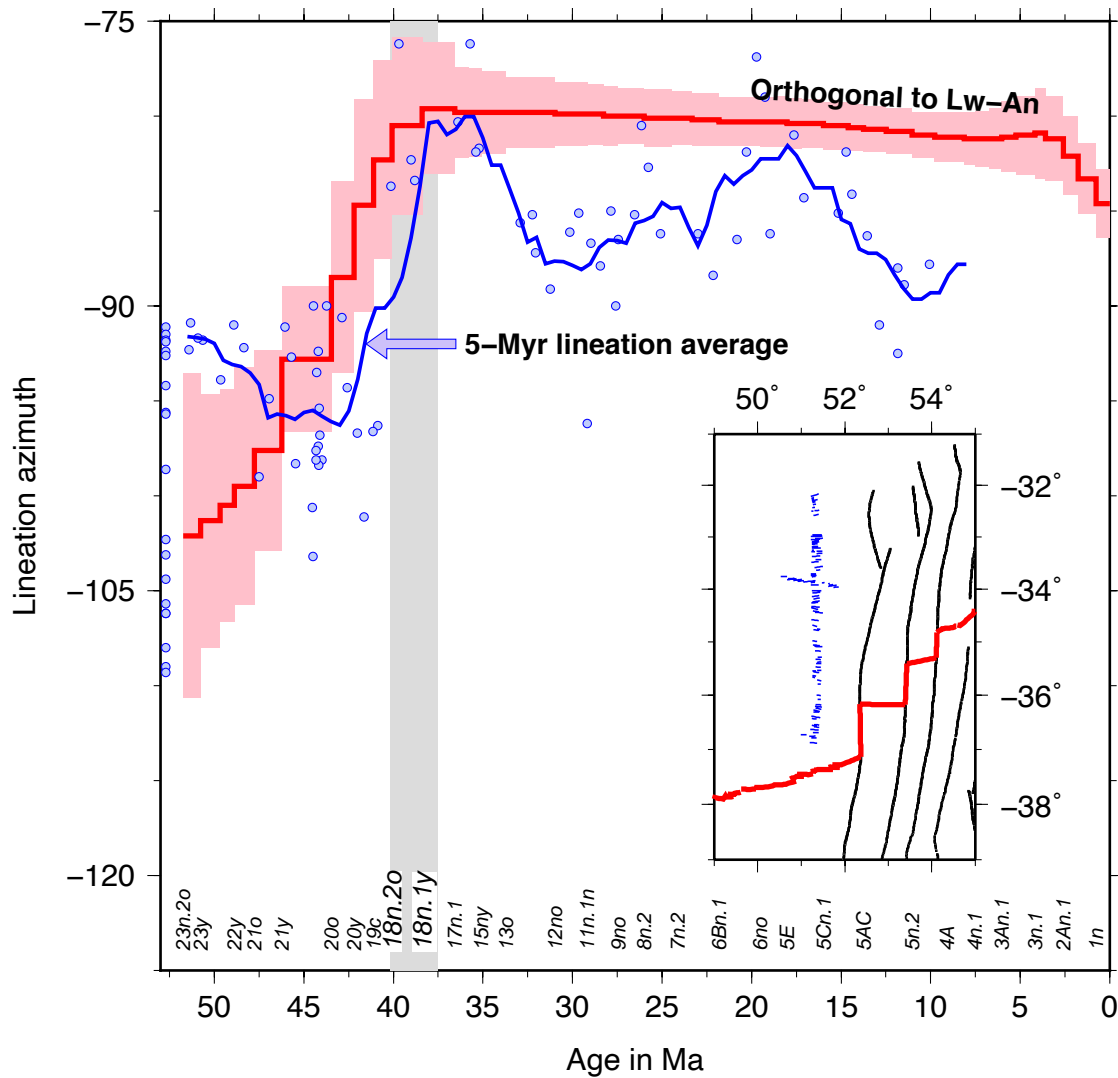
Supplemental Figure 3. Observed (black) and predicted (colored) Nubia-Antarctic fracture zone traces. The red lines and lines that are color coded by seafloor age show the flow lines determined respectively from the best-fitting and noise-reduced Nubia-Antarctica rotation sequences in Tables 2 and 3 of the main document. Vertical distances are exaggerated by ≈ 3 times relative to horizontal distances to emphasize the misfits and noise in the digitized traces. Positive and negative distances on the horizontal axis indicate parts of the fracture zone that lie on the Africa or Antarctica sides of the SWIR, respectively. Distances are measured relative to the locations of the northern and southern ridge-transform fault intersections (RTI), where each fracture zone begins. Transform faults, which are located between the northern and southern RTIs, are omitted from this plot.



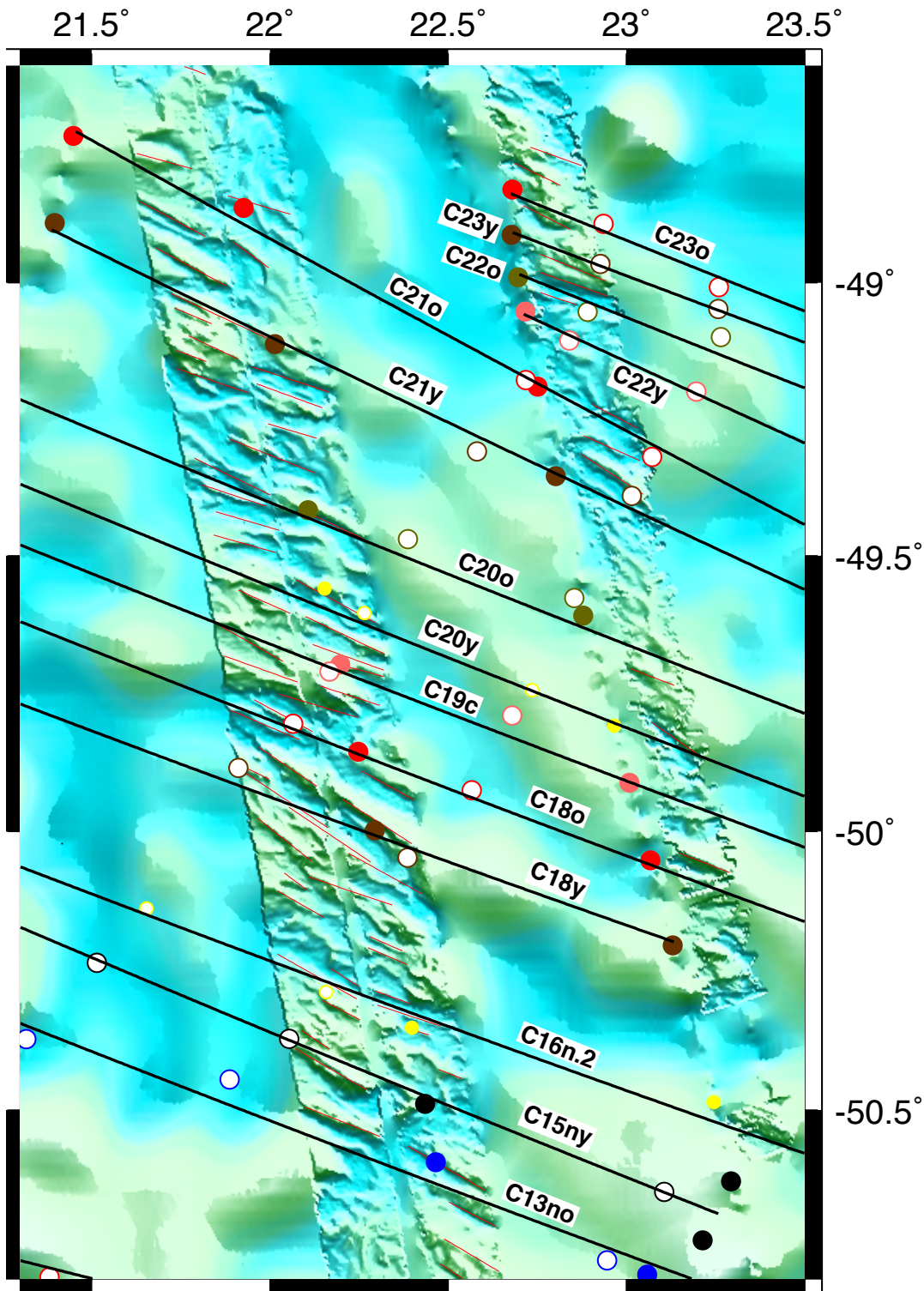
Supplemental Figure 4. Observed (black) and predicted (colored) Lwandle-Antarctic fracture zone traces. The red lines and lines that are color coded by seafloor age show the flow lines determined respectively from the noise-mitigated and best-fitting Lwandle-Antarctica rotation sequences in Tables 5 and 6 of the main document. Vertical distances are exaggerated by 5 times relative to horizontal distances to emphasize the misfits and noise in the digitized traces. Positive and negative distances on the horizontal axis indicate parts of the fracture zone that lie on the Africa or Antarctica sides of the SWIR, respectively. Distances are measured relative to the locations of the northern and southern ridge-transform fault intersections (RTI), where each fracture zone begins. Transform faults, which are located between the northern and southern RTIs, are omitted from this plot.



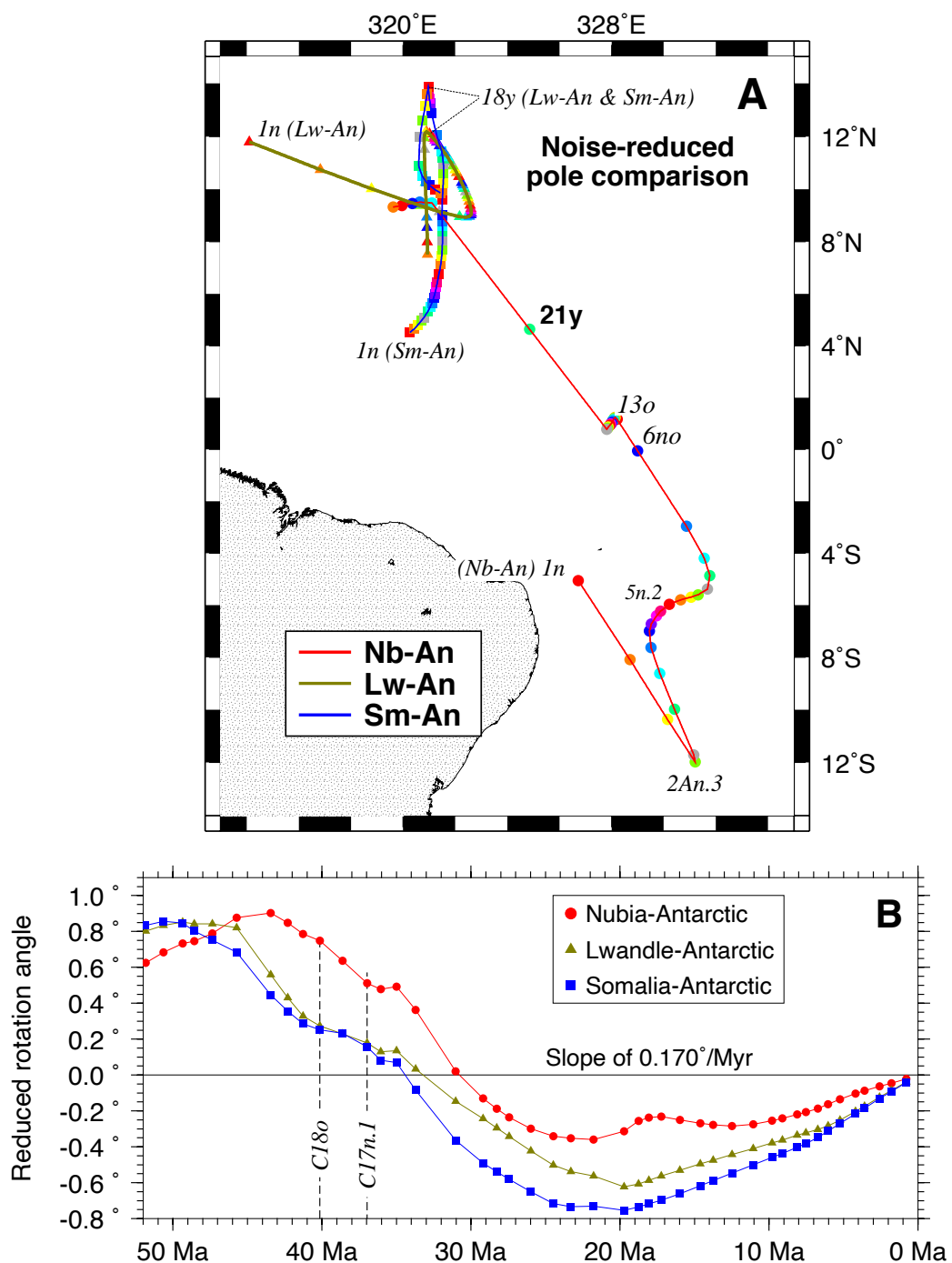
Supplemental Figure 5. Observed (black) and predicted (colored) Somalia-Antarctic fracture zone traces. The red lines and lines that are color coded by seafloor age show the flow lines determined respectively from the best-fitting and noise-reduced Nubia-Antarctica rotation sequences in Tables 8 and 9 of the main document. Vertical distances are exaggerated by 2.6 times relative to horizontal distances to emphasize the misfits and noise in the digitized traces. Positive and negative distances on the horizontal axis indicate parts of the fracture zone that lie on the Africa or Antarctica sides of the SWIR, respectively. Distances are measured relative to the locations of the northern and southern ridge-transform fault intersections (RTI), where each fracture zone begins. Transform faults, which are located between the northern and southern RTIs, are omitted from this plot.



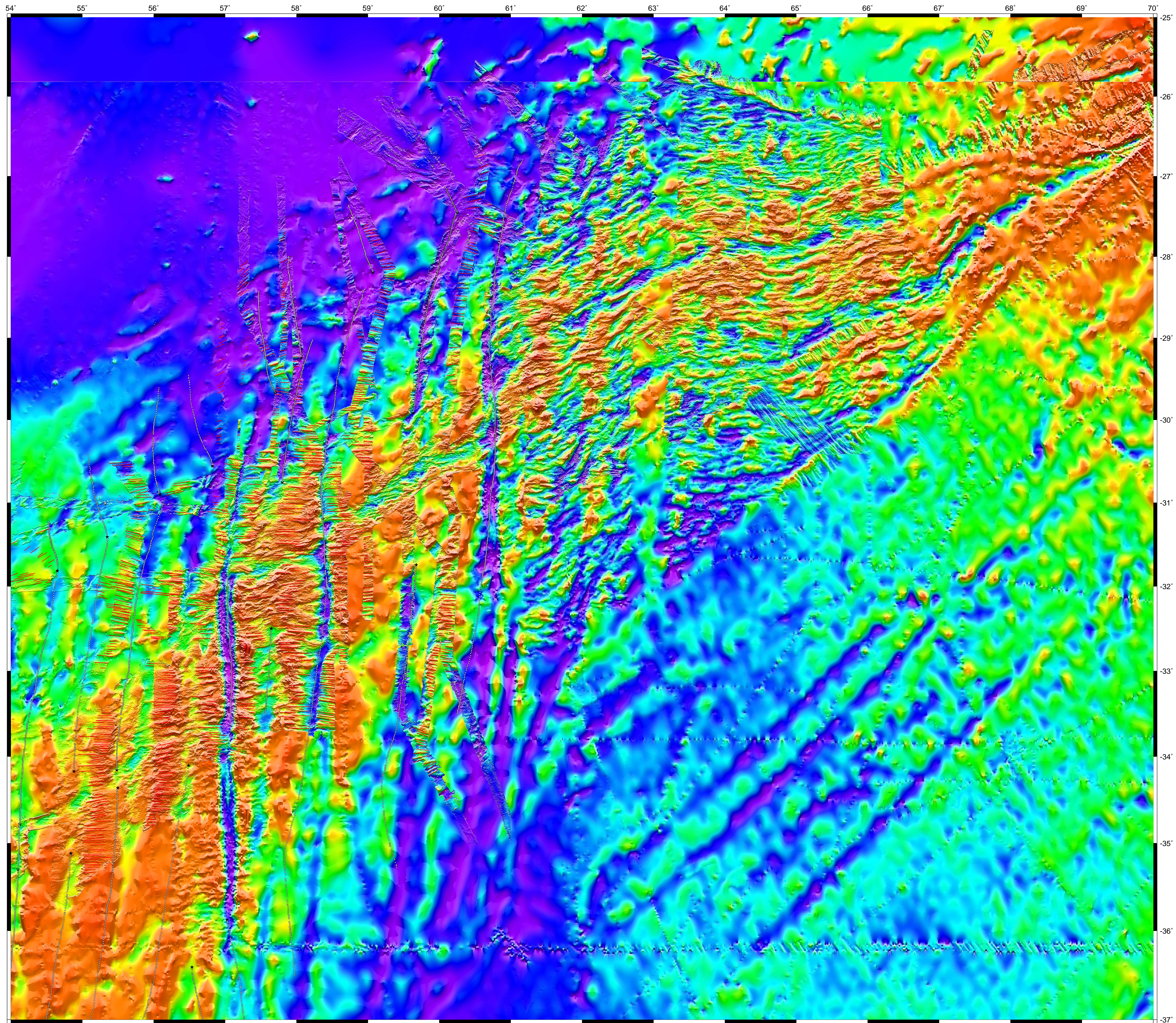
Supplemental Figure 6. Individual and average abyssal hill azimuths (circles and blue line respectively) versus seafloor age for a multibeam transect at 51°E north of the Lwandle-Antarctic portion of the Southwest Indian Ridge. The blue lines in the inset map show the abyssal hill lineations we digitized from the R/V Gallieni multibeam data. The average abyssal hill azimuths were determined at 0.5-Myr intervals for 5-Myr-long periods centered on each time. The bold red line shows directions that are orthogonal to Lwandle-Antarctic plate slip directions predicted by noise-reduced rotations from Table 7 of the main document.



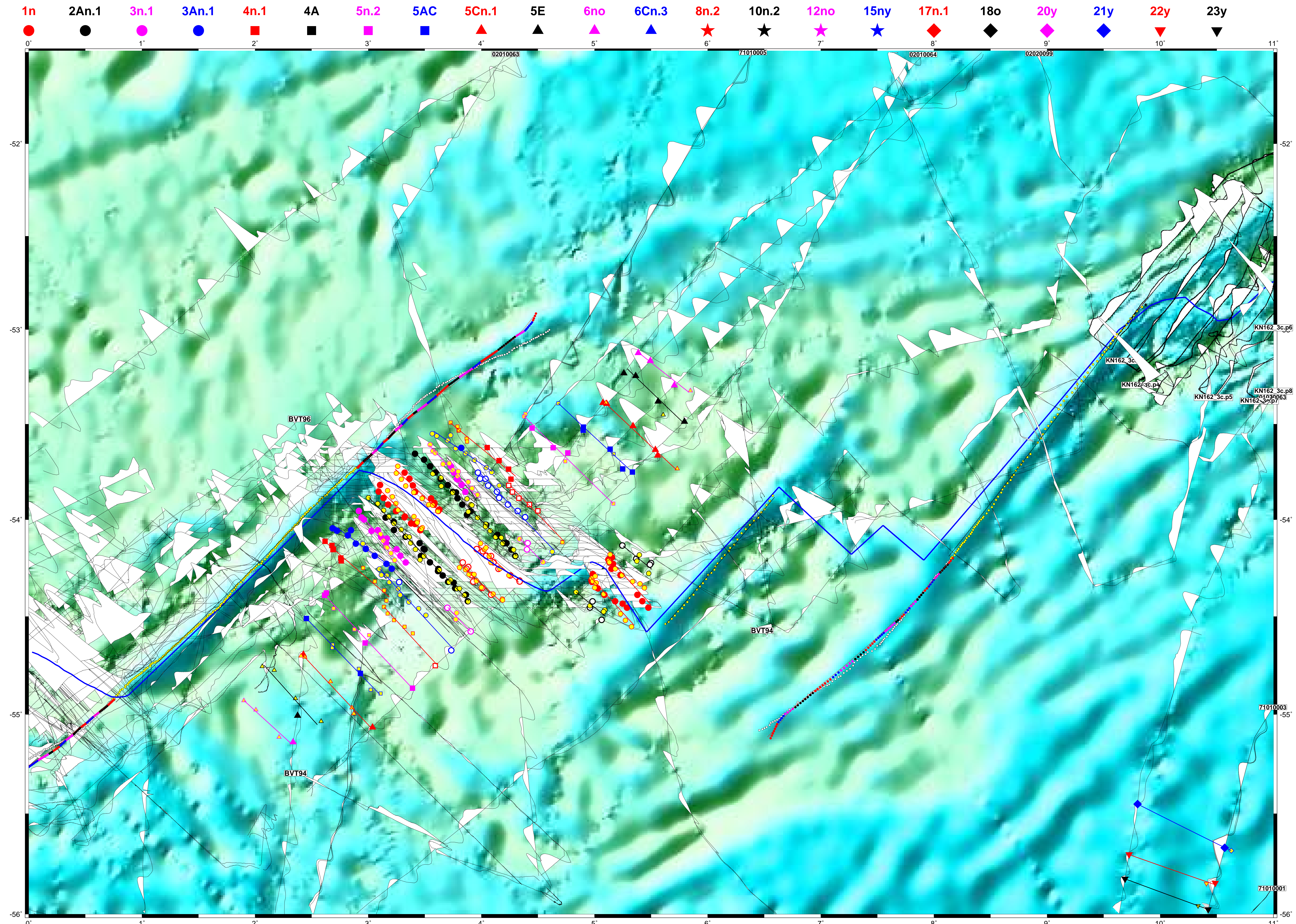
Supplemental Figure 7. Nubia plate seafloor bathymetry and reconstructed magnetic lineations, Chrons 23 to 13, for the region identified in the inset map in Fig. 4 of the main document. Any rotation of the abyssal hill fabric between C19c and C18y (41.1 to 38.4 Ma) is modest (less than 10 degrees), in contrast to a much larger change in the Somalia-Antarctic abyssal hill fabric during this period (Fig. 14 of the main document). The circles show our magnetic reversal identifications in place (filled) or rotated from the Antarctic plate (open). Black lines are the great circles that best fit each ensemble of stationary and rotated reversal crossings.



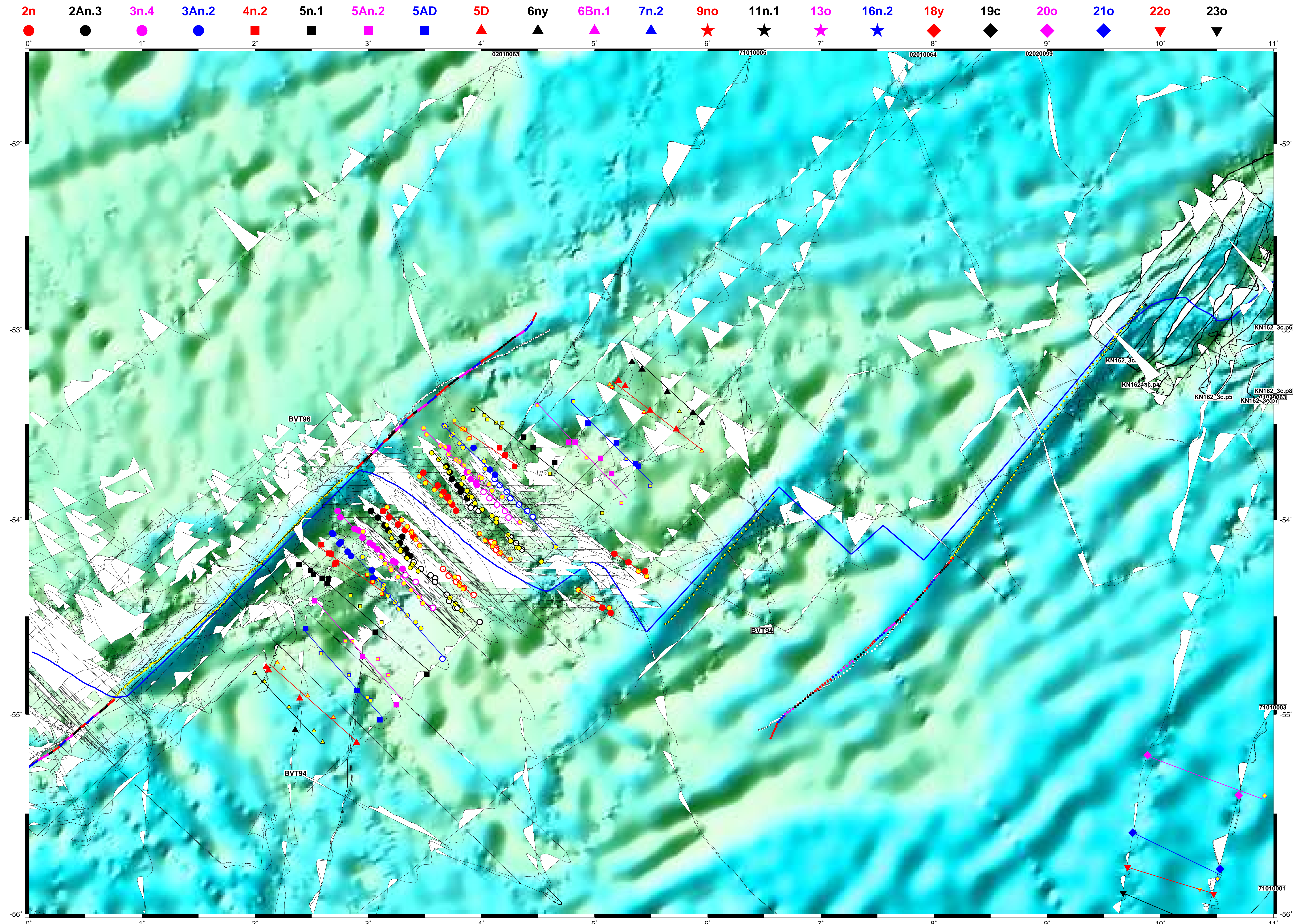
Supplemental Figure 8. Comparisons of Nubia-Antarctic (Nb-An), Lwandle-Antarctic (Lw-An), and Somalia-Antarctic (Sm-An) noise-reduced finite rotation poles (A) and opening angles (B), C1n to C23o. Confidence ellipses are omitted for clarity. All the opening angles are reduced by a slope of $0.170^\circ \text{ Myr}^{-1}$ to facilitate a comparison of their angular rate changes. The same pole and angle sequences are shown in more detail in Figures 3, 7, and 11 of the main document.



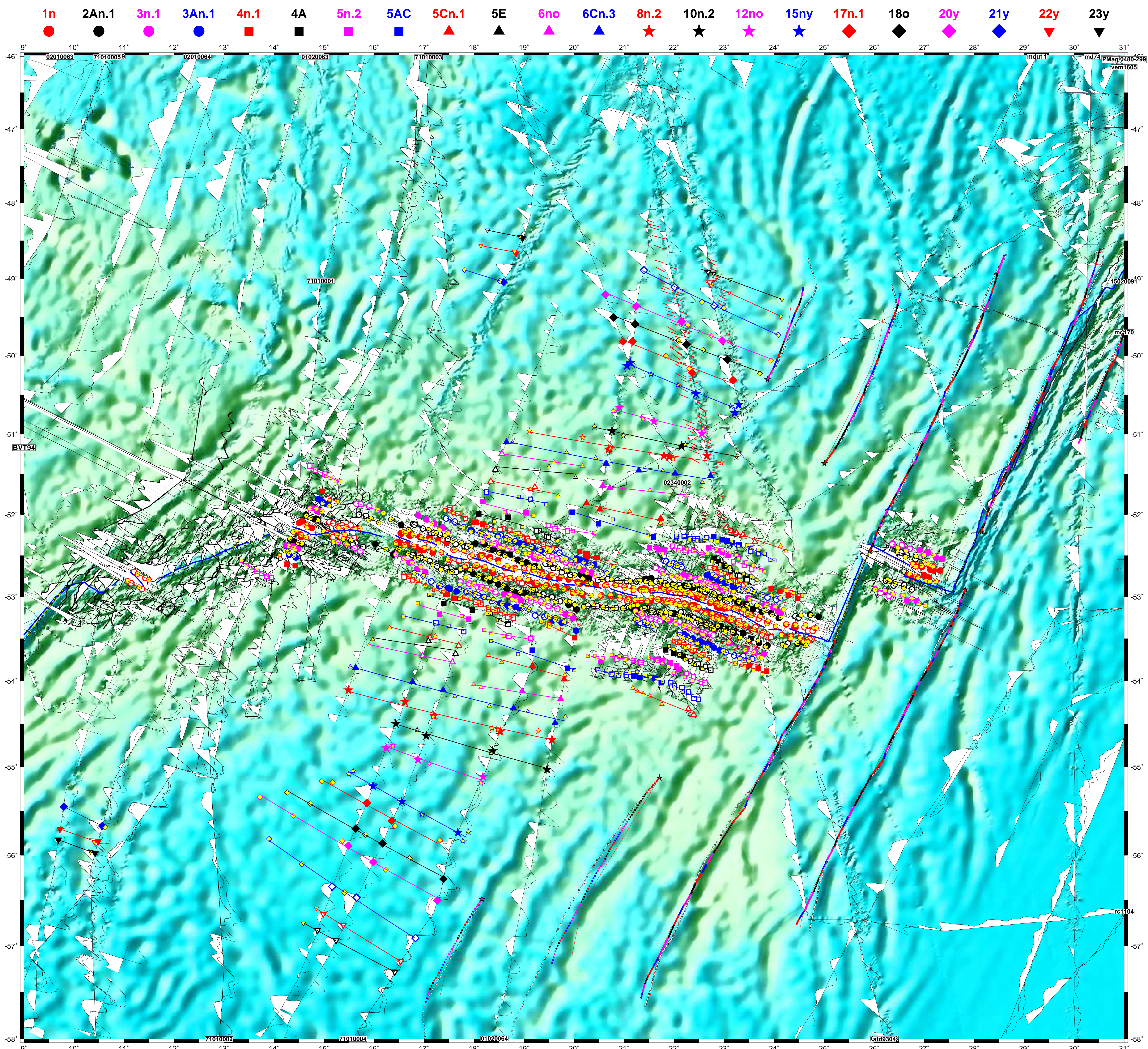
Supplemental Figure 9. Blended bathymetric grids with French and other multibeam observations that were used in our analysis. Circles identify the digitized fracture zone crossings that constrain our rotations and red lines show abyssal hill lineations used in part of our analysis. The resolutions of the underlying multibeam grids included in this map range from ~150 to 500 meters.



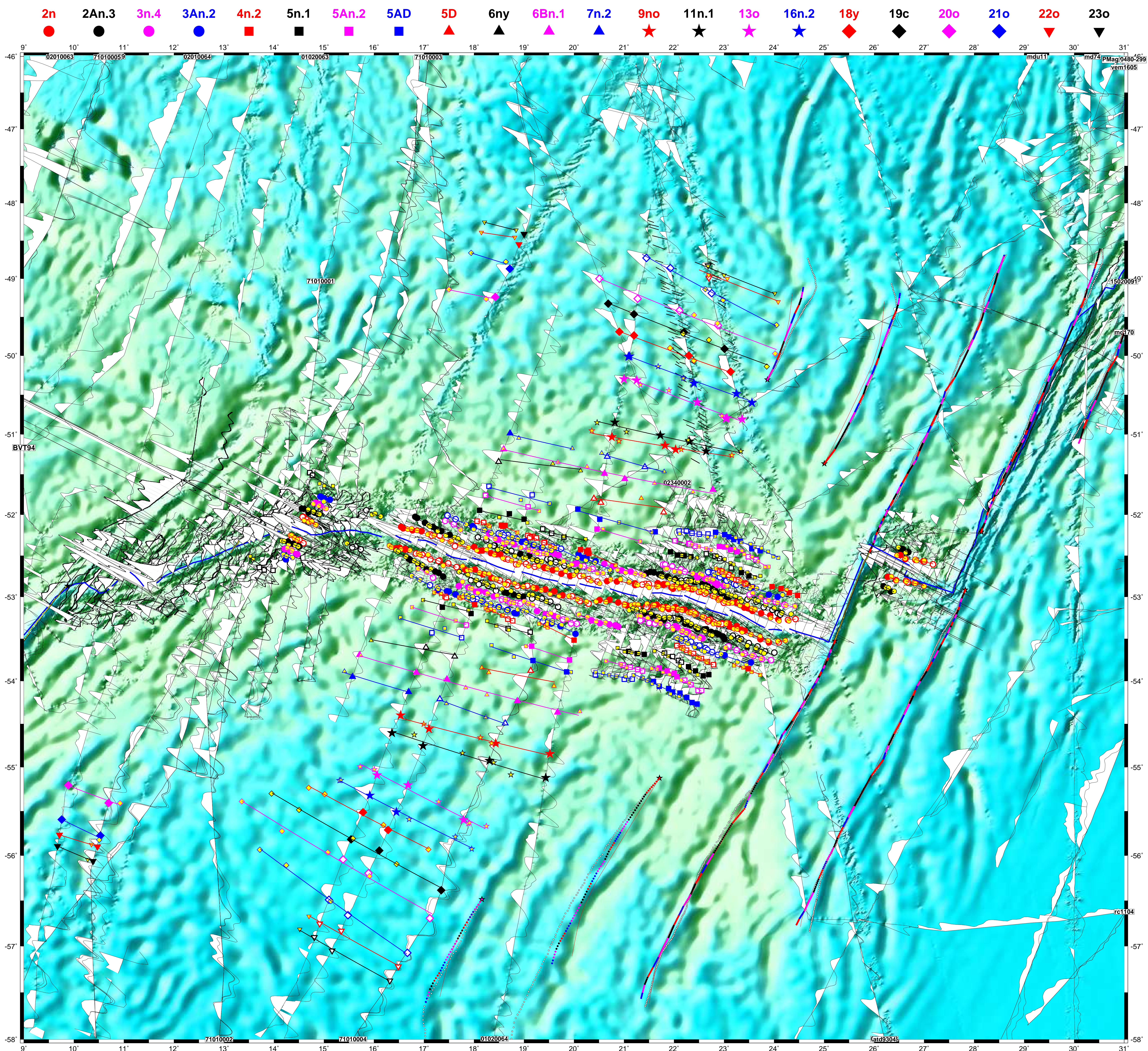
Supplemental Figure 10. Along-track magnetic anomaly observations, magnetic reversal identifications, and reconstructed magnetic lineations for the magnetic reversals identified in the legend above the figure. The map base is 1-minute seafloor bathymetry from topex.ucsd.edu/WWW_html/mar_topo.html (Smith and Sandwell 1997). Fracture zone flow lines digitized from GeoMapApp are indicated by the tiny white circles. Flow lines predicted with the best-fitting and noise-mitigated Nubia-Antarctic rotations (Tables 2 and 3) are indicated by the colored circles and red lines, respectively. The symbols that are filled with yellow show magnetic reversal crossings rotated onto their same-age counterparts across the ridge. The solid symbols and white-filled symbols are magnetic reversal crossings in their original locations. The colored lines are the great circles that best fit the stationary and rotated reversal crossings for each paleo-spreading segment. Digitized transform faults are indicated by circles with black rims and yellow cores. Transform fault small circles that are predicted by the Chron 1n pole are shown by the thin black lines.



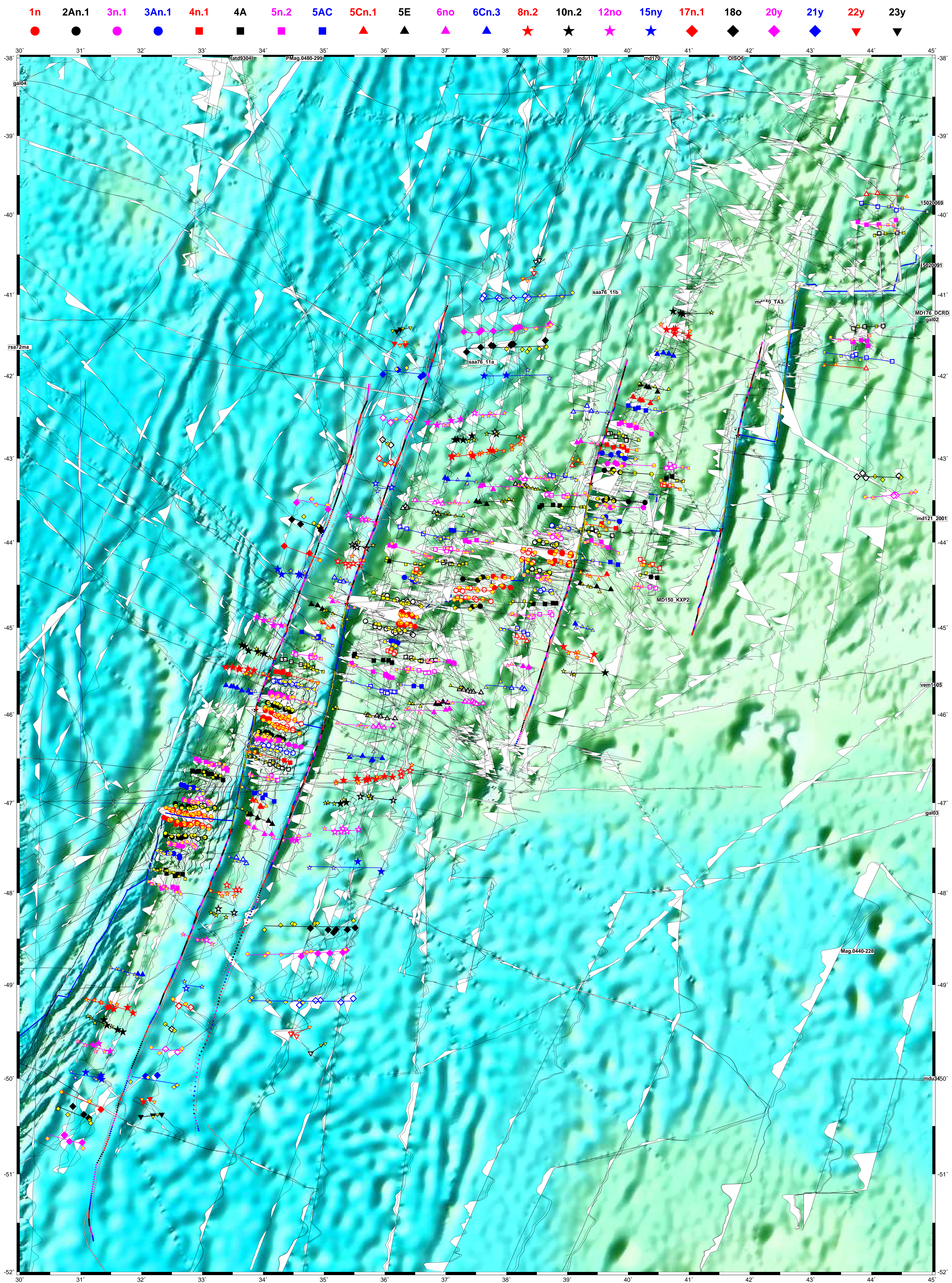
Supplemental Figure 11. Along-track magnetic anomaly observations, magnetic reversal identifications, and reconstructed magnetic lineations for the magnetic reversals identified in the legend above the figure. The map base is 1-minute seafloor bathymetry from topex.ucsd.edu/WWW_html/mar_topo.html (Smith and Sandwell 1997). Fracture zone flow lines digitized from GeoMapApp are indicated by the tiny white circles. Flow lines predicted with the best-fitting and noise-mitigated Nubia-Antarctic rotations (Tables 2 and 3) are indicated by the colored circles and red lines, respectively. The symbols that are filled with yellow show magnetic reversal crossings rotated onto their same-age counterparts across the ridge. The solid symbols and white-filled symbols are magnetic reversal crossings in their original locations. The colored lines are the great circles that best fit the stationary and rotated reversal crossings for each paleo-spreading segment. Digitized transform faults are indicated by circles with black rims and yellow cores. Transform fault small circles that are predicted by the Chron 1n pole are shown by the thin black lines.



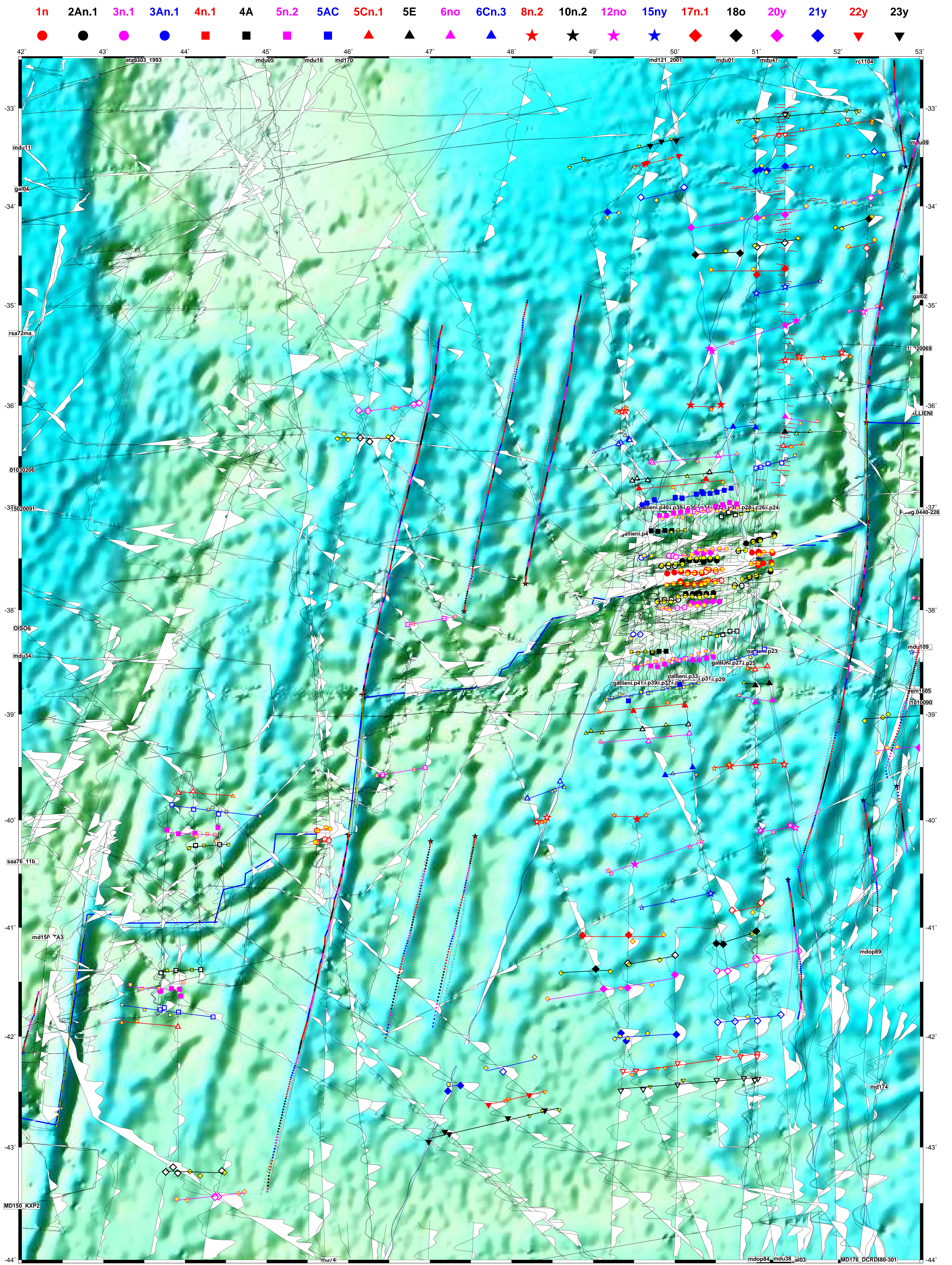
Supplemental Figure 12. Along-track magnetic anomaly observations, magnetic reversal identifications, and reconstructed magnetic lineations for the magnetic reversals identified in the legend above the figure. The map base is 1-minute seafloor bathymetry from topex.ucsd.edu/WWW_html/mar_topo.html (Smith and Sandwell 1997). Fracture zone flow lines digitized from GeoMapApp are indicated by the tiny white circles. Flow lines predicted with the best-fitting and noise-mitigated Nubia-Antarctic rotations (Tables 2 and 3) are indicated by the colored circles and red lines, respectively. The symbols that are filled with yellow show magnetic reversal crossings rotated onto their same-age counterparts across the ridge. The solid symbols and white-filled symbols are magnetic reversal crossings in their original locations. The colored lines are the great circles that best fit the stationary and rotated reversal crossings for each paleo-spreading segment. Digitized transform faults are indicated by circles with black rims and yellow cores. Transform fault small circles that are predicted by the Chron 1n pole are shown by the thin black lines.



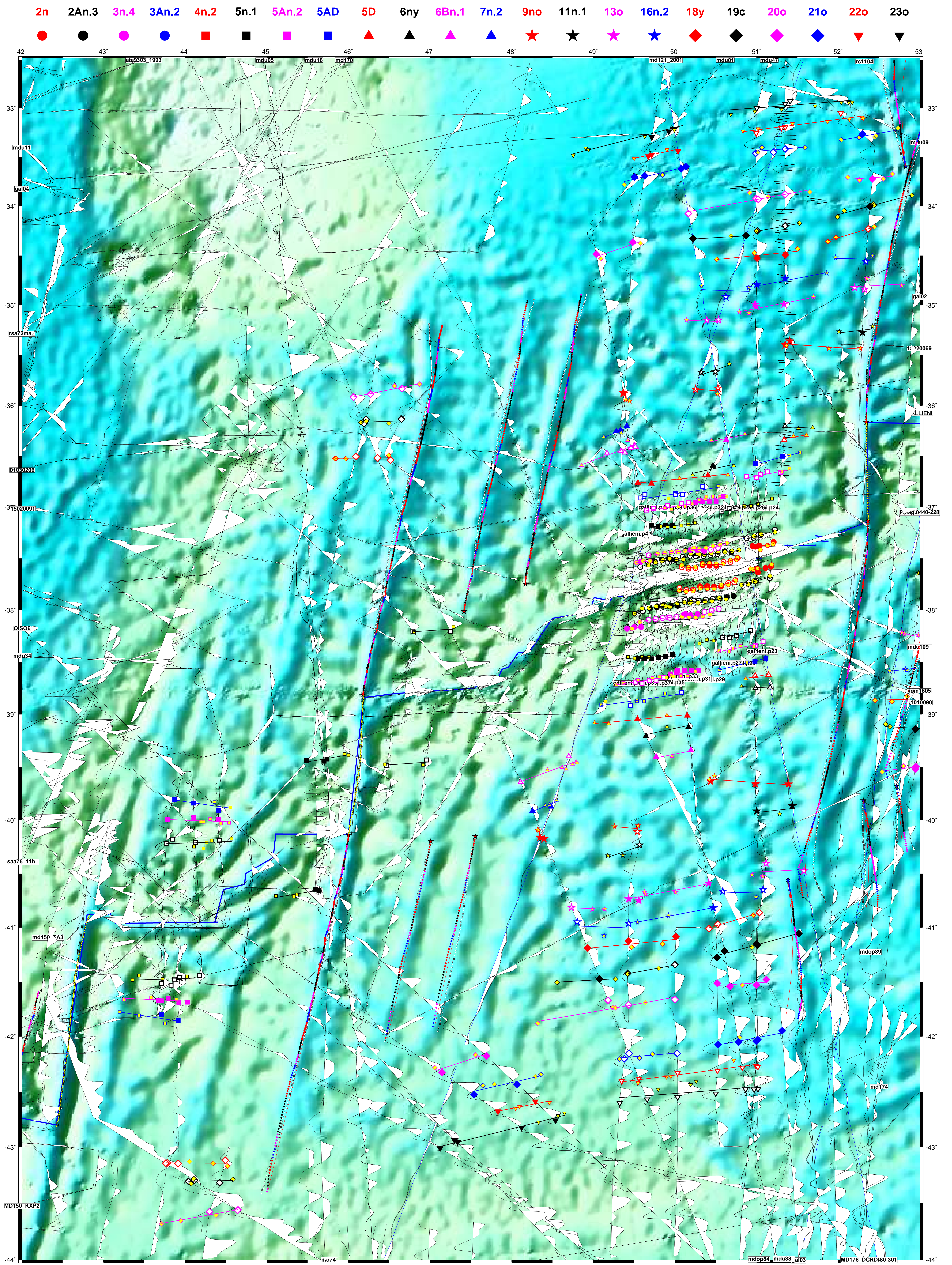
Supplemental Figure 13. Along-track magnetic anomaly observations, magnetic reversal identifications, and reconstructed magnetic lineations for the magnetic reversals identified in the legend above the figure. The map base is 1-minute seafloor bathymetry from topex.ucsd.edu/WWW_html/mar_topo.html (Smith and Sandwell 1997). Fracture zone flow lines digitized from GeoMapApp are indicated by the tiny white circles. Flow lines predicted with the best-fitting and noise-mitigated Nubia-Antarctic rotations (Tables 2 and 3) are indicated by the colored circles and red lines, respectively. The symbols that are filled with yellow show magnetic reversal crossings rotated onto their same-age counterparts across the ridge. The solid symbols and white-filled symbols are magnetic reversal crossings in their original locations. The colored lines are the great circles that best fit the stationary and rotated reversal crossings for each paleo-spreading segment. Digitized transform faults are indicated by circles with black rims and yellow cores. Transform fault small circles that are predicted by the Chron 1n pole are shown by the thin black lines.



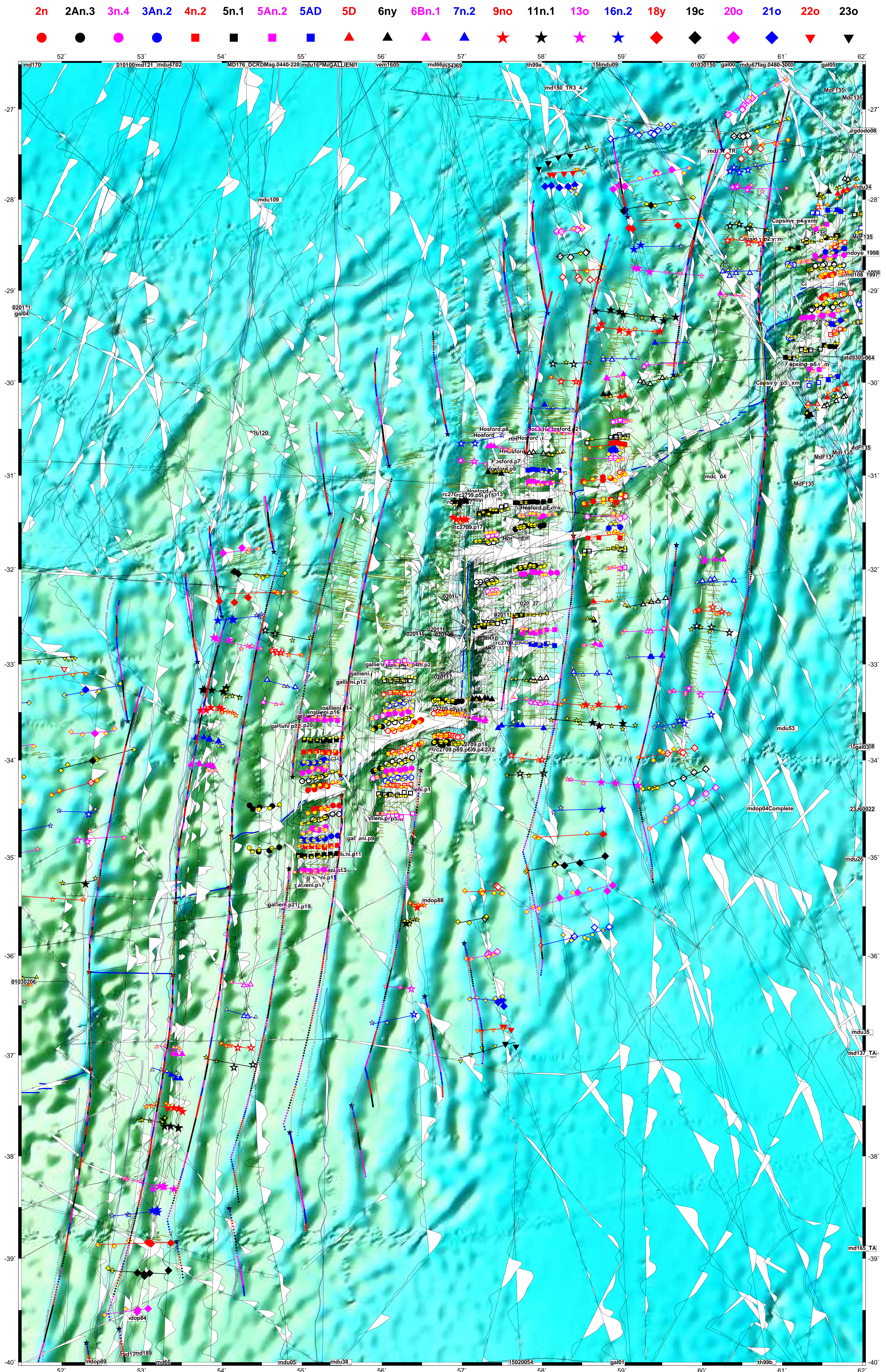
Supplemental Figure 14. Along-track magnetic anomaly observations, magnetic reversal identifications, and reconstructed magnetic lineations for the magnetic reversals identified in the legend above the figure. The map base is 1-minute seafloor bathymetry from topex.ucsd.edu/WWW_html/mar_topo.html (Smith and Sandwell 1997). Fracture zone flow lines digitized from GeoMapApp are indicated by the tiny white circles. Flow lines predicted with the best-fitting and noise-mitigated Lwandle-Antarctic rotations (Tables 5 and 6) are indicated by the colored circles and red lines, respectively. The symbols that are filled with yellow show magnetic reversal crossings rotated onto their same-age counterparts across the ridge. The solid symbols and white-filled symbols are magnetic reversal crossings in their original locations. The colored lines are the great circles that best fit the stationary and rotated reversal crossings for each paleo-spreading segment. Digitized transform faults are indicated by circles with black rims and yellow cores. Transform fault small circles that are predicted by the Chron 1n pole are shown by the thin black lines.



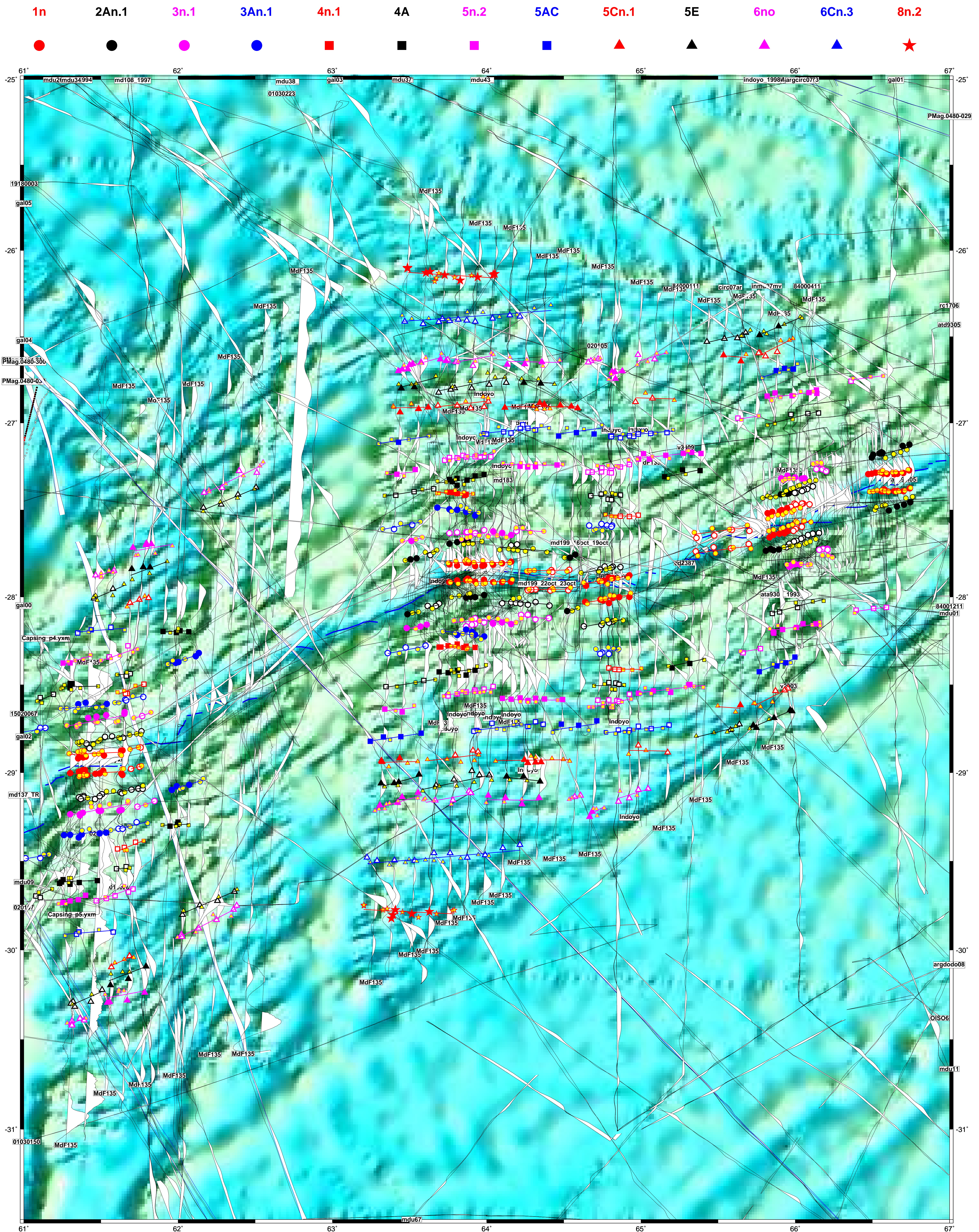
Supplemental Figure 16. Along-track magnetic anomaly observations, magnetic reversal identifications, and reconstructed magnetic lineations for the magnetic reversals identified in the legend above the figure. The map base is 1-minute seafloor bathymetry from topex.ucsd.edu/WWW_html/mar_topo.html (Smith and Sandwell 1997). Fracture zone flow lines digitized from GeoMapApp are indicated by the tiny white circles. Flow lines predicted with the best-fitting and noise-mitigated Lwandle-Antarctic rotations (Tables 5 and 6) are indicated by the colored circles and red lines, respectively. The symbols that are filled with yellow show magnetic reversal crossings rotated onto their same-age counterparts across the ridge. The solid symbols and white-filled symbols are magnetic reversal crossings in their original locations. The colored lines are the great circles that best fit the stationary and rotated reversal crossings for each paleo-spreading segment. Digitized transform faults are indicated by circles with black rims and yellow cores. Transform fault small circles that are predicted by the Chron 1n pole are shown by the thin black lines.



Supplemental Figure 17. Along-track magnetic anomaly observations, magnetic reversal identifications, and reconstructed magnetic lineations for the magnetic reversals identified in the legend above the figure. The map base is 1-minute seafloor bathymetry from topex.ucsd.edu/WWW_html/mar_topo.html (Smith and Sandwell 1997). Fracture zone flow lines digitized from GeoMapApp are indicated by the tiny white circles. Flow lines predicted with the best-fitting and noise-mitigated Lwandle-Antarctic rotations (Tables 5 and 6) are indicated by the colored circles and red lines, respectively. The symbols that are filled with yellow show magnetic reversal crossings rotated onto their same-age counterparts across the ridge. The solid symbols and white-filled symbols are magnetic reversal crossings in their original locations. The colored lines are the great circles that best fit the stationary and rotated reversal crossings for each paleo-spreading segment. Digitized transform faults are indicated by circles with black rims and yellow cores. Transform fault small circles that are predicted by the Chron 1n pole are shown by the thin black lines.



Supplemental Figure 19. Along-track magnetic anomaly observations, magnetic reversal identifications, and reconstructed magnetic lineations for the magnetic reversals identified in the legend above the figure. The map base is 1-minute seafloor bathymetry from topex.ucsd.edu/WWW_html/mar_topo.html (Smith and Sandwell 1997). The small colored circles show the predicted fracture zone flow lines created with the Lwandle-Antarctic rotations west of 52°E (Table 5) and Somalia-Antarctic rotations east of 52°E (Table 8). Flow lines predicted with the Lwandle-Antarctic and Somalia-Antarctic noise-mitigated rotations (Tables 6 and 9, respectively) are indicated by the red lines. The symbols that are filled with yellow show magnetic reversal crossings rotated onto their same-age counterparts across the ridge. The solid symbols and white-filled symbols are magnetic reversals in their original locations. The colored lines are the great circles that best fit the stationary and rotated reversal crossings for each paleo-spreading segment. Digitized transform faults are indicated by circles with black rims and yellow cores. Transform fault small circles that are predicted by the Chron 1n pole are shown by the thin black lines. The olive-colored lines show abyssal hill lineations digitized from multibeam tracks and discussed in the text.



Supplemental Figure 20. Along-track magnetic anomaly observations, magnetic reversal identifications, and reconstructed magnetic lineations for the magnetic reversals identified in the legend above the figure. The map base is 1-minute seafloor bathymetry from topex.ucsd.edu/WWW_html/mar_topo.html (Smith and Sandwell 1997). The magnetic reversals shown in the figure are reconstructed with best-fitting Somalia-Antarctic rotations from Table 8. The symbols that are filled with yellow show magnetic reversal crossings rotated onto their same-age counterparts across the ridge. The solid symbols and white-filled symbols are magnetic reversal crossings in their original locations. The colored lines are the great circles that best fit the stationary and rotated reversal crossings for each paleo-spreading segment.

